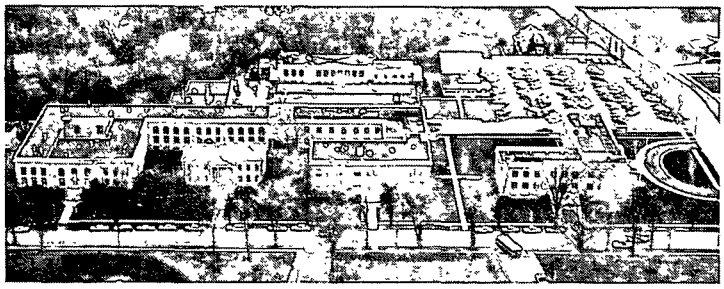

THE INSTITUTE OF PAPER CHEMISTRY, APPLETON, WISCONSIN

IPC TECHNICAL PAPER SERIES

NUMBER 309

ONE DIMENSIONAL MATHEMATICAL MODEL OF BLACK LIQUOR GASIFIER

N. T. SHIANG AND T. M. GRACE

NOVEMBER, 1988

One Dimensional Mathematical Model of Black Liquor Gasifier

N. T. Shiang and T. M. Grace

This manuscript is based on results obtained in IPC research and is to be presented at the AIChE Annual Meeting in Washington, DC in December, 1988

ONE DIMENSIONAL MATHEMATICAL MODEL OF BLACK LIQUOR GASIFIER

N. T. Shiang and T. M. Grace
The Institute of Paper Chemistry
P.O. Box 1039
Appleton, WI 54912

ABSTRACT

A one-dimensional mathematical model for black liquor gasification has been developed which incorporates recently acquired fundamental information on black liquor behavior. The model was used to examine the performance of a pressurized gasifier operating in two very distinct modes. The first case is for a gasifier fired with 1-5 mm diameter liquor drops moving countercurrently to the gas flow. The second case is for very small 10-100 micron liquor drops moving cocurrently with the gases. The model was used to examine the effects of liquor solids content, air/solids ratio, drop size and size distribution on gasifier performance.

The performance of the cocurrent gasifier is dominated by material balance and chemical equilibrium considerations. The countercurrent gasifier showed interesting behavior. There is a very high peak in the temperature profile which can be made to occur near the center of the gasifier. The heating value (dry basis) of the exit gas is not a function of the initial liquor solids content. In contrast, the cocurrent case requires an external heat input to get the heating value (dry basis) of the exit gas independent of the initial liquor solids content.

INTRODUCTION

Coal gasification reactors are contacting devices in which coal reacts with air-steam or oxygen-steam gas mixtures. The reactors are designed to convert as large a fraction of the coal as possible to combustible gases, for direct use in power generation, for chemical feedstock, or for upgrading to substitute natural gas. Gasification reactors can be classified into categories according to the particle size and the method of contacting between the gas and solid.

Large size coal (6-50 mm) and moderate operating temperature require long residence times (hours) in fixed or moving beds. One example is the Lurgi reactor which runs with dry ash in the bottom and so the maximum temperature is limited by the ash fusion temperature. The Lurgi reactor requires a minimum steam-to-oxygen ratio of approximately seven because of the low temperature operation. In a slagging reactor, the maximum temperature is much higher, and the steam-to-oxygen ratio is approximately one (1). Fludized bed gasifiers operate with residence times of minutes and with smaller coal size (500-1000 micron) but at lower temperatures to avoid defluidization. Highly pulverized coals (1-150 micron) are used in entrained systems with very high operating temperatures that result in very short residence time (1 s). Coal gasifiers are discussed in several review books (2,3).

Black liquor gasification has been studied by Champion International and Rockwell International for several years (4,5,6,7). Bench scale tests showed that black liquor could be successfully gasified to generate fuel gas with a heating value of 5000 KJ/m^3 while producing smelt with a high reduction ratio (>95%). A subsequent pilot scale test was not as successful due to high radiative heat loss to the surroundings. As a result of the pilot scale tests, a countercurrent firing technique with particle size between 1 and 5 mm was suggested by Rockwell (7).

Several typical sets of bench scale test results with air as the oxidant were presented by Champion International and Rockwell International (4,5). All of the tests ran smoothly at constant temperature with continuous black liquor feed and product gas removal. The black liquor gasified readily in a molten salt. The high heating value (HHV) of dry product gas ranged from 3148 to 6008 kJ/m^3 for runs without oil addition and correlated with the air/black liquor feed ratio. No SO_2 was detected. H_2S concentrations varied from about 0.08 to 0.25% by volume. Particulate loadings ranged from 3.6 to 9.6 g/m^3 (1.6-4.2 gr/scf). Melt reduction of sulfate to sulfide was generally over 90%. Residual carbon in the melt was generally less than 0.1%. Product gas compositions in these tests were in reasonable agreement with equilibrium predictions. One test with oxygen generated a product gas with HHV as high as 9700 KJ/m^3.

The high heating value of dry product gas is a strong function of, and decreases with, air/black liquor (65% solids content) weight ratio as seen in Figure 1. Equilibrium coupled with stoichiometry predicts the gas heating value over a wide range of conditions in both bench and pilot tests. The air/liquor weight ratio has to be kept as low as 1.1 in order to meet the minimum requirement of 4500 KJ/m^3 specified by turbine manufacturers. The 1.1 air/liquor weight ratio corresponds to a 1.7 air/dry liquor weight ratio, or 0.35 of the stoichiometric ratio needed to combust the black liquor completely.

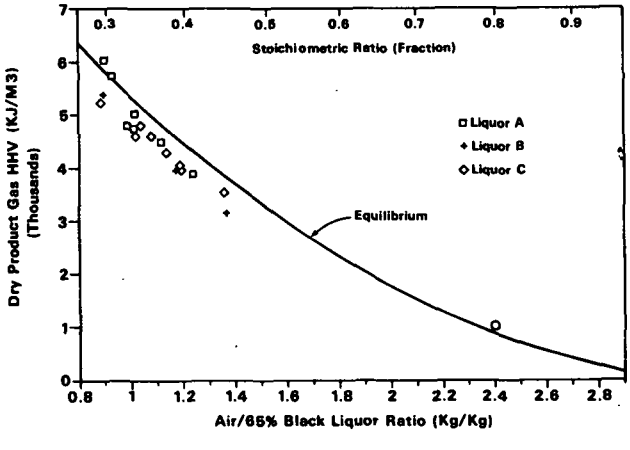

Figure 1. Heating value of fuel gas.

Kelleher (7) showed the sulfur reduction efficiency increased with $CO/(CO+CO_2)$ mole ratio, and decreased with the air/liquor weight ratio. Most

runs with poor reduction efficiency came from pilot tests (6,7) which required a stoichiometric ratio as high as 0.8 to maintain isothermal operation at 900-1050°C with the high reactor heat losses. The test data indicated that in the range of product gas compositions projected for a commercial plant, sulfate reduction over 90% can be expected.

MATHEMATICAL MODELING

Although the experimental gas compositions are in reasonable agreement with stoichiometry and equilibrium calculations, little insight is gained about temperature and concentration profiles in the reactor or the effect of liquor particle size on gasifier performance. A one dimensional mathematical model for black liquor was developed and used to evaluate two cases:

(1) Air in plug flow countercurrent to relatively coarse black liquor particles.

(2) Air in cocurrent with fine black liquor particles.

The first case is a partial simulation of the Rockwell molten salt gasifier while the second simulates some aspects of cyclone gasifiers.

Countercurrent Case

Air is introduced at the bottom of the gasifier and passes upward in countercurrent plug flow against black liquor particles which are sprayed down from the top of the gasifier. The black liquor particles go through 4 stages; drying, pyrolysis, char burning, and sulfide oxidation, as shown by Hupa (8). The mathematical modeling of each stage is described below. For simplicity, it is assumed that no sodium fume and sulfur emissions are generated during either combustion or gasification. Chemical equilibria is assumed in the gas phase so that only the transfer of elements rather than chemical species from particles to gas needs to be treated. Heat transfer in the axial direction is neglected.

Particle Drying

Below 150°C, the particle temperature increases with time as heat is absorbed from the surroundings by means of radiation and convection. Once the particle temperature reaches 150°C, it remains for the entire drying phase. The particle diameter during the drying phase is assumed to be 30% greater than its original value. The mathematical model is shown below:

$$d(M_p*C_{ps}*T_p)/dt = Q_{gp} \qquad \text{for } T_p < 150°C$$

$$d(M_p)/dt = 0. \qquad \text{for } T_p < 150°C$$

$$-d(M_p)/dt = Q_{gp}/i_w \qquad \text{for } T_p = 150°C$$

Where $Q_{gp} = A_p*[h*(T_g-T_p)+ \beta(T_g^4-T_p^4)]$

M_p = particle mass

T_p = particle temperature

T_g = gas temperature

i_w = latent heat of water

h = convective heat transfer coefficient = $Nu*k_f/D_p$

Nu = Nusselt Number = $2. + 0.6*Re^{0.5}*Pr^{0.333}$

k_f = thermal conductivity of gas phase

C_{ps} = particle specific heat

D_p = particle diameter

A_p = particle surface area

The Ackerman correction factor is used to calculate the impeding effect of mass transfer due to either water vaporization or pyrolysis gas on the convective heat transfer coefficient.

Particle Pyrolysis

Although black liquor pyrolysis is much more complicated than either drying or char burning, it is not too difficult to model the global phenomena, i.e., weight loss. Iatridis and Gavalas (9) have studied pyrolysis of a precipitated kraft lignin at 400-700°C with rapid heating rate of 400°C/sec and found the ultimate weight loss at high temperature is about 70% of dry lignin. This is consistent with recent research work at The Institute of Paper Chemistry (10), and corresponds to a 35% weight loss of dry black liquor solids (combustible organics are about one half of total solids). The activation energy is calculated to be 9.7 kcal/g mole which is quite close to the value of 7.8 kcal/mole reported by Kubes (11) for black liquor. Kulas (12) presented an empirical correlation equation for volatiles burning which shows the rate as a function of particle diameter and oxygen concentration but not the gas temperature. Her data cover gas temperatures between 660 and 860°C, initial drop diameters between 2-4 mm, and oxygen contents between 0 and 21%. This correlation equation cannot be applied to particle diameters greater than 5 mm.

We have used the following algorithm for particle weight loss during pyrolysis:

$$-d(M_p)/dt = k_p*(M_p-M_{p*}) \qquad \text{for } T_p < 500°C$$

Where M_{p*} = ultimate weight loss

$= M_s*(1.3593-1.66\times10^{-3}*T_p+9.75\times10^{-7}*T_p^2)$

M_s = particle dry weight

$k_p = 68.2*\exp(-9.7\times10^3/R/T_p)$

And

$$-d(M_p)/dt = M_s*(0.1634/D_{pi}+0.34*X_o/D_{pi}-0.54*X_o-0.316) \qquad \text{for } T_p > 500°C$$

Where D_{pi} = particle initial diameter in cm

X_o = oxygen content in fraction

The energy balance is made around the particle, as

follows:

$$d(M_p*C_{pp}*T_p)/dt = Q_{gp}$$

Where C_{pp} = specific heat of dry particle

The particle diameter is assumed to increase linearly with weight loss during pyrolysis, as shown below:

$$D_p/D_{pi} = 1 + (M_s-M_p)/0.35/M_s*(Swell-1)$$

Where Swell = diameter swelling factor, greater than one.

Char Gasification

Kraft char burns via a sulfate/sulfide cycle as described by Grace (13). The carbon in the char reacts with sulfate, reducing it to sulfide and forming CO_2 and CO. The sulfide in turn reacts with oxygen from the combustion air, reforming sulfate and completing the cycle. The sulfate/sulfide cycle acts to carry oxygen to the carbon which is burnt off. The importance of the sulfate/sulfide cycle is that it permits simultaneous sulfate reduction and carbon burnup in the presence of an oxygen-containing atmosphere as long as the rate limiting step during char burning is oxygen mass transfer to the burning char. The carbon burning rate through the sulfate/sulfide cycle is determined either by oxygen mass transfer rate if sulfate reduction is complete, or by sulfate-carbon reaction kinetics if reduction efficiency is a little below 100%. The carbon in char can also be gasified by CO_2 or H_2O. The char-CO_2 reaction has been studied by Goerg and Cameron (14) in excess molten salt as well as by Li (15) using thermogravimetry. Kinetic constants for char-CO_2 reaction in this model are taken from Li. Generally, the char-CO_2 reaction is much slower than char-O_2 reaction. Since no kinetic expression was available for char-H_2O reaction, it was ignored. The rate for the char-H_2O reaction is expected to be about the same as the char-CO_2 reaction.

The total char gasification rate is given by

$$-d(M_{cb})/dt = r_{cyc} + r_{co2}$$

Where M_{cb} = carbon mole in kraft char

r_{cyc} = cycle burning rate

$= 2/(2-fco)*ro$ for RR = 1

$= 4/(2-f_{co})*rs$ for RR < 1

r_{co2} = char-CO_2 reaction rate, $8.02*\exp(-44.7\times10^3/R/T_{pk})*M_{cb}*C_{co2}/(10^{-6}+0.91*C_{co2}+0.53*C_{co})$

ro = oxygen mass transfer rate, $k_o*A_p*C_o$

rs = sulfate reduction rate, $k_s*M_{cb}*\exp(-29200/R/T_{pk})$

f_{co} = CO fraction in CO and CO_2 mixture

k_o = oxygen diffusional coefficient

C_o, C_{co}, C_{co2} = oxygen, CO, CO_2 mole concentration

k_s = char-sulfate rate constant

The carbon monoxide and carbon dioxide concentrations are those at the surface of the kraft char particle and can be calculated from the balances between mass transfer rates and kinetic rates.

The sulfate reduction ratio is determined from a sulfide material balance as shown below:

$$N_{na}*s*d(RR)/dt = r_s-r_o/2$$

Where s = sulfidity, mole S/mole Na2

N_{na} = mole Na_2 in kraft char

The particle mass M_p during burning is related to both carbon mass and reduction ratio by

$$M_p = N_{na}*(106.*(1-s)+142*s*(1-RR)+78*s*RR) + 12*M_{cb}$$

The heat accumulation on char particles is the balance among the heat of reaction for carbon burning through the sulfate-sulfide cycle, carbon reacting with CO_2, the heat of reaction for sulfide oxidation and heat exchange between gas and particle:

$$d(M_p*C_{pp}*T_p)/dt = Q_{gp} - \Delta H_{cyc}*r_{cyc} + \Delta H_{rr}*N_{na}*s*dRR/dt - \Delta H_{co2}*r_{co2}$$

Where ΔH_{cyc}, ΔH_{co2} = heat of reaction for carbon burning through sulfate-sulfide cycle and char-CO2 reaction, respectively, cal/g mole

ΔH_{rr} = Heat of reaction for sulfide oxidation, cal/g mole

The heat of reaction is evaluated as the difference between the sum of enthalpy of products and the sum of enthalpy of reactants at the corresponding particle or gas temperatures.

The particle diameter reaches a maximum at the end of pyrolysis, then decreases with the amount of char gasified. The final particle diameter is about 70% of the original diameter based on a specific gravity of 2 for smelt.

$$D_p/D_{pi} = Swell - (M_{cbo}-M_{cb})/M_{cbo}*(Swell-0.7)$$

Where M_{cbo} = initial carbon mole in kraft char after pyrolysis.

Particle Trajectory

The equation of motion for black liquor particle can be expressed as follows:

$$M_p*dU_p/dt = M_p*g - C_d*A_p'*\rho_g*Abs(U_p-U_g)*(U_p-U_g)/2.$$

Where C_d = drag coefficient

$= 24/Re*(1+0.15*Re^{0.687})$ for $1 < Re < 10^3$

$= 0.44$ for $10^3 < Re$ (Newton's law)

A_p' = particle projected area

g = gravity constant

Subscripts p, g refer to particle and gas, respectively.

The equation for the drag coefficient is taken from Wallis (16). Although it contains no correction for the reduction of drag due to devolatilization, this equation is typical of those for solid spheres, and widely used in particle momentum balances (17).

Gas Phase

Direct minimization of Gibbs free energy is used to determine the composition of seven chemical species, N_2, O_2, CO, CO_2, H_2, H_2O, CH_4 in equilibria. The temperature and compositions in the gas phase are updated during each iteration by keeping track of the mass and energy transport between particles and gas phase through drying, pyrolysis, gasification and oxidation phases.

(1) Drying

$$dG_H/dx = -\sum_i (dM_p/dt)_i*(dt/dx)_i*2/18$$

$$dG_O/dx = -\sum_i (dM_p/dt)_i*(dt/dx)_i*1/18$$

$$dH_{pg}/dx = -\sum_i ((dM_p/dt)*H_{p,H2O} + Q_{gp})_i * (dt/dx)_i$$

(2) Pyrolysis

$$dG_C/dx = -\sum_i (dM_p/dt)_i*(dt/dx)_i*XV_C$$

$$dG_H/dx = -\sum_i (dM_p/dt)_i*(dt/dx)_i*XV_H$$

$$dG_O/dx = -\sum_i (dM_p/dt)_i*(dt/dx)_i*XV_O$$

$$dH_{pg}/dx = -\sum_i ((dM_p/dt)*HV + Q_{gp})_i * (dt/dx)_i$$

(3) Char gasification and sulfide oxidation

$$dG_C/dx = -\sum_i (dM_{cb}/dt)_i*(dt/dx)_i$$

$$dG_O/dx = \sum_i (4*N_{na}*s*dRR/dt)_i*(dt/dx)_i$$

$$dH_{pg}/dx = \sum_i (r_{co2}*(2.*H_{p,co}-H_{g,co2}) + r_{cyc}*DH_{cyc} + 2*N_{na}*s* dRR/dt*H_{g,o2} - Q_{gp})_i * (dt/dx)_i$$

Where $DH_{cyc} = f_{co}*(H_{p,co}-.5*H_{g,o2}) + (1-f_{co})*(H_{p,co2}-H_{g,o2})$

G = elemental atom flow from particles to gas phase

H_{pg} = enthalpy transport from particles to gas phase

XV = volatiles elemental compositions

x = gasifier distance

H_p, H_g = enthalpy of compound evaluated at particle and gas temperatures, respectively.

subscript C, H, O refer to carbon, hydrogen, oxygen atoms.

subscript i refers to different black liquor particles.

(dt/dx) is determined by particle flight trajectory.

The elemental composition (XV) and enthalpy (HV) of volatiles are calculated from elemental analysis and bomb heating value analysis of dry liquor by making the following assumptions:

(1) kraft char consists of only carbon in the organic portion.

(2) volatiles have constant composition and account for 35% weight loss during pyrolysis.

The assumption of only carbon and inorganics in the char avoids the ambiguity on defining the enthalpy state of kraft char. Each elemental flow rate in the gas phase at any point of gasifier is the sum of the element from the combustion air and total transport of the element between particles and gas phase from the air ports up to that point. A small amount of CO_2 and moisture is assumed in the combustion air to avoid the computation error due to zero elemental flow. The computation starts with specified temperature and concentration profiles. The elemental and enthalpy transport from particles to the gas phase are calculated for each gas zone during the particle flight trajectories. The gas temperature and concentration are then updated from the equilibrium calculations with a relaxation parameter as low as 0.1 to maintain stability and speed to reach the convergence of the solution. The thermodynamic data of Gibbs free energy and enthalpy are taken from JANAF Thermochemical Tables (18). The calculations of physical properties of the gas phase mixture are based on the equations recommended by Reid (19), and updated once on each gas zone.

Cocurrent Flow

Black liquor particles in the range of 10-100 micron are introduced either upward or downward in cocurrent flow with the oxidizing gas. Although the gasifier consists of three stages - drying, pyrolysis, and char gasification, the rates of drying and pyrolysis are so fast relative to gasification that most of gasifier is used for char gasification.

Gas-particle equilibria are assumed during gasification for all elements except carbon. The carbon gasification rate is determined by char-CO_2 reaction kinetics and mass transfer rate. The char-O_2 is much less important due to rapid depletion of oxygen during the pyrolysis/volatile burning stage. The equilibria assumption is justified for the fine particles because the contact surface area between gas and particle is so great that gas and particle temperatures reach the same value in a very short

period of time. The assumption of equilibria between gas and particles makes it possible to predict the sulfur and sodium emissions from the gasifier for the cocurrent case. Four chemical species (Na_2CO_3, Na_2S, Na_2SO_4, NaOH) are assumed in the liquid phase. Gas phase consists of four additional species H_2S, SO_2, Na, NaOH besides seven species mentioned before. Most of the equations used for cocurrent flow are the same as these used for countercurrent flow and are not repeated here.

MODEL CALCULATIONS - COUNTERCURRENT CASE

There are many design variables for a commercial black liquor gasifier, including flow rates, oxidant/liquor weight ratio, liquor solids content, solids heating value, oxidant temperature, oxygen concentration, pressure, gasifier geometry, mean drop diameter, and drop diameter distribution. The gasifier design and operating conditions proposed by Kohl (6,7) summarized in Table 1 serve as the base for the countercurrent case. Relatively large liquor drops, between 1 and 5 mm in diameter, are used for this countercurrent case.

Effect of Particle Size

Figure 2 shows the gas and particle temperature distribution throughout the gasifier with particles falling countercurrent to the gas flow. The peak temperatures are much greater than the adiabatic flame temperature (1500°C), since:

(1) All liquid water is vaporized and carried away with the gas before the particles reach the region at peak temperatures and the water vapor has much greater heat capacity than either nitrogen or carbon dioxide does.

(2) A large amount of heat is released during the oxidation of sodium sulfide to sulfate after most kraft char is either gasified or combusted.

(3) The countercurrent flow pattern tends to preheat the black liquor particles by cooling the exit gas and preheat air by cooling the exit smelt, thus hot reactants are brought into the peak temperature region.

The gas temperature is hotter than the particle temperature in the part of the gasifier between liquor spray nozzle and the peak temperature region. The particle temperature is greater than the gas temperature between the air entrance and the peak temperature region. Particle size has a significant effect on the temperature distribution. Particles with a diameter below 1.5 mm are entrained into the bulk gas flow and never reach the bottom of the gasifier. Particles greater than 4 mm are not dried during the flight trajectories. The location of peak temperatures moves downward from 35% of the gasifier height for 2 mm particles to the bottom of the gasifier for 3 mm particles. For a particle size greater than 3 mm, so much unpyrolyzed material lands on the bottom (oxygen depletion is so fast that no oxygen rich combustion is observed) and so little preheat of the combustion air occurs that the magnitude of peak temperature drops rapidly.

Table 1. Operating conditions and geometry of gasifier.

Gasifier diameter (m)	2.4
Gasifier height (m)	12.2
Gasifier pressure (atm)	15
Black liquor feed rate (kg/hr)	29000
Black liquor solids content (%)	70
Black liquor temperature (°C)	110
Liquor diameter swelling factor	3.0
Air/black liquor solids mass ratio	1.7
Air temperature (°C)	400
Black liquor HHV (KJ/kg)	14784
Elemental composition Na/S/C/H/O	0.19/0.045/0.36/0.042/0.363

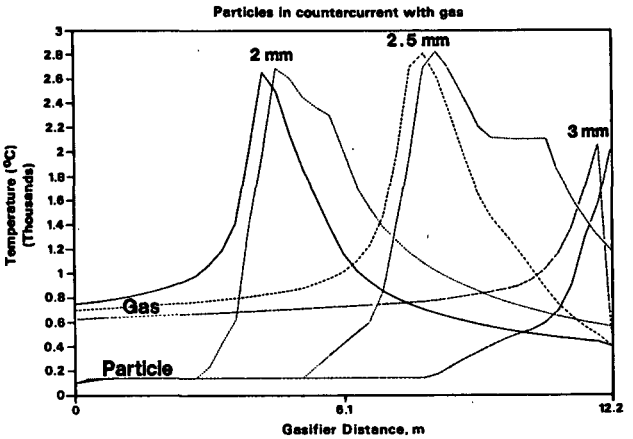

Figure 2. Gas, particle temperature distribution.

Figure 3 shows the sulfate reduction efficiency as a function of particle size. (A reduction efficiency of 50% was arbitrarily chosen for the starting liquor.) Although the reduction efficiency temporarily reaches 100% for particles smaller than about 2.7 mm, the sulfide eventually is oxidized to sulfate due to the rapid depletion of carbon. The 3 mm particles land on the bottom fully reduced. The 3.5 mm particles landing on the bottom have temperatures too low to drive the sulfide-sulfate cycle and so retain their initial reduction value. The range of particle sizes allowing complete sulfur reduction could be so (a spread of about 0.5 mm) that it might not be realistic for commercial operations. However, this behavior is significantly changed if multisize particles are fired instead of monosize particles.

Figure 4 shows the gas concentration distribution throughout the gasifier for 2.5 mm particles. The peak temperature shown in Figure 2 takes place where oxygen is almost depleted as shown in Figure 4. Carbon dioxide is the dominant carbon species if oxygen is present. More carbon monoxide is pro-

duced through char-CO_2 gasification after the depletion of oxygen, and CO reaches a maximum value somewhere in the gasifier after which the water-gas shift reaction (producing CO_2 and H_2) becomes more significant due to vaporization of water from the incoming particles. Several percent of methane is produced at the exit of gasifier due to low temperatures.

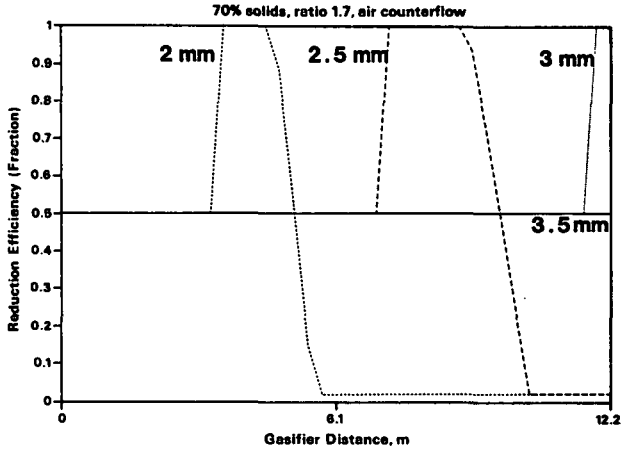

Figure 3. Sulfate reduction efficiency.

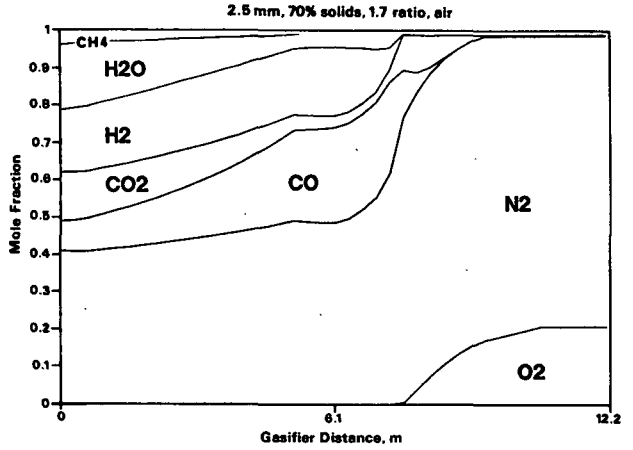

Figure 4. Gas concentration distribution.

Figure 5 shows the dry gas heating value distribution throughout the gasifier with particle size as the paramèter. The 2 mm and 2.5 mm particles generate the highest dry HHV of fuel gas at the exit since all sodium sulfide is oxidized to sulfate. The 3 mm particles give the lowest HHV due to 100% reduction efficiency. The 3.5 mm particles give the medium value because 50% reduction efficiency is assumed for the feed liquor. All the information in Figures 2 through 5 is consistent.

Effect of Air/Solids Ratio

Figure 6 shows the effect of air/solids ratio on gas temperature and heating value distributions throughout the countercurrent gasifier. The peak gas temperature shifts toward the liquor inlet with increasing air/solids ratio. The heating value of the exit gas decreases with increasing air/solids ratio in accordance with equilibrium/stoichiometric predictions. Although it is desirable to use lower air/solids ratios to generate fuel gas with greater HHV, the necessary gasifier length increases as the air/solids ratio decreases. This calculation suggests that it may be possible to use a ratio as low as 1.3 in the base case gasifier to obtain a HHV 30% greater than that obtained with the design ratio of 1.7.

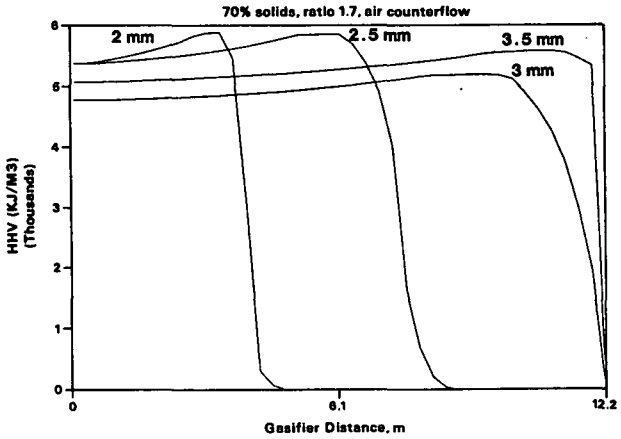

Figure 5. Dry gas heating value distribution.

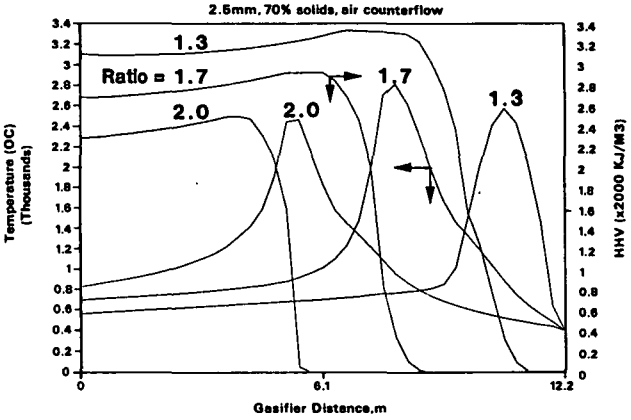

Figure 6. Effect of air/solids ratio.

Effect of Solids Content

Figure 7 shows that the HHV of the exit gas increases slightly with increasing black liquor solids content. This is because less water-shift reaction occurs in the gas phase near the top of the gasifier with higher solids content liquor. Figure 8 shows the gas concentration distribution for 100% solids content feed. There is almost no change in carbon monoxide and hydrogen concentration in the upper gasifier, in contrast to the behavior in Figure 4 with 70% solids content feed. Inlet liquor solids content has only a minor effect on temperature profiles. The HHV of the exit fuel gas is not very sensitive to the solids content of black liquor feed. This is an important advantage of countercurrent over cocurrent operation.

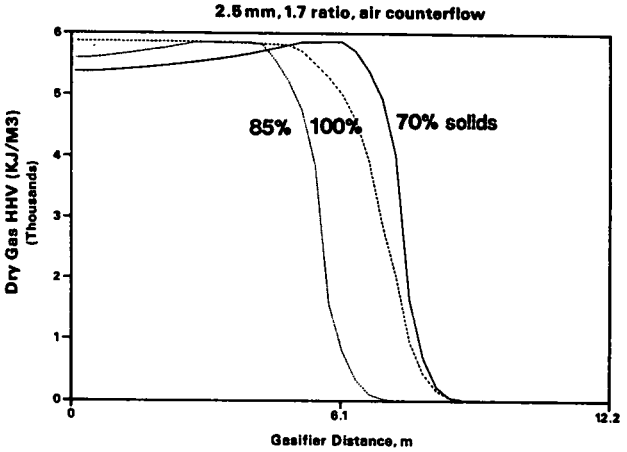

Figure 7. Effect of solids content on HHV distribution.

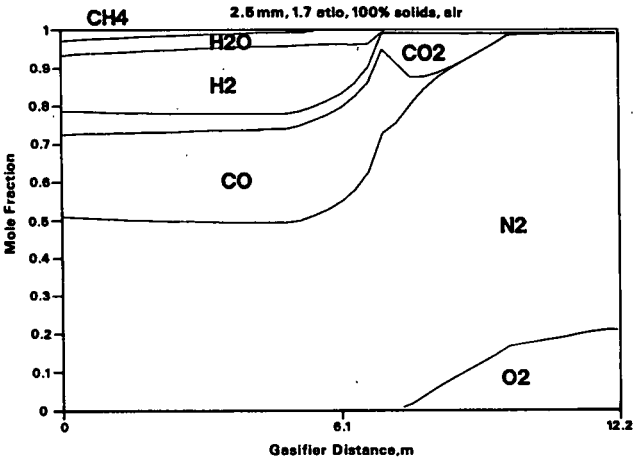

Figure 8. Effect of solids content on gas concentration.

Effect of Liquor Drop Size Distribution

Figure 9 shows the effect of drop size distribution on temperature profiles. The liquor is introduced as equal mass fractions of four different drop sizes, 2, 2.5, 3, and 3.5 mm. The gas temperature profile together with four particle temperature profiles is shown in Figure 9. Comparison with Figure 2 shows significant differences in behavior between monosize and multidisperse drops. The peak temperature for the multisize distribution occurs near the end of gasifier and is lower than that for the monosize distribution. The temperature profile of the smallest particles (2 mm) is much closer to that of the gas phase than that for the larger particles (3 and 3.5 mm).

Figure 10 shows the effect of size distribution on the reduction efficiency. Note that the small particles have their reduction efficiency maintained at 100% throughout the lower gasifier due to the protection of the large particles which consumes most of the free oxygen during char burning in the lower gasifier. A high overall reduction efficiency is not as difficult to achieve as it is with a monosize distribution.

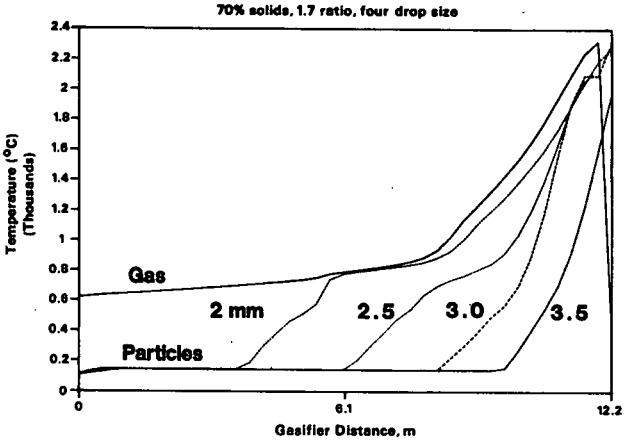

Figure 9. Effect of size distribution on temperature profiles.

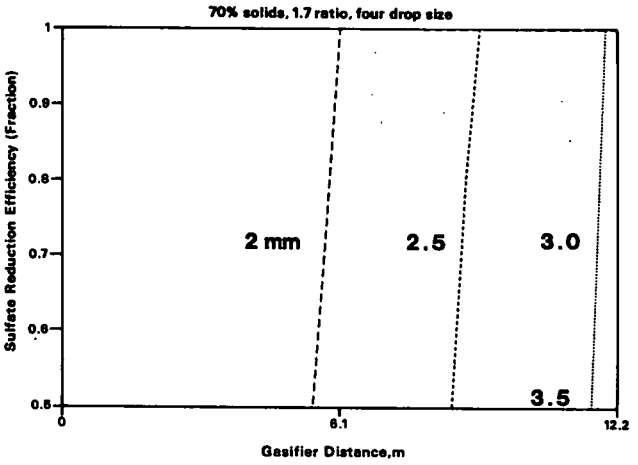

Figure 10. Effect of size distribution on reduction efficiency.

MODEL CALCULATIONS - COCURRENT CASE

The cocurrent case uses the same dimensions and pressure as the countercurrent case. However, fine particles with diameters between 10 and 100 microns are chosen since particle entrainment is not an issue.

Effect of Solids Content and Particle Size

Figure 11 shows the temperature profile for three different solids content. The particle and gas temperatures are practically identical after a very short distance so only the gas temperature is shown. Differences in particle size between 10 and 100 micron have no effect on the gasifier performance so no specific particle size is given in Figure 11. The maximum temperature occurs near the entrance. The temperature then decreases along the gasifier mainly due to the reaction of carbon with carbon dioxide. Most of the oxygen in the input air is consumed very close to the entrance so that the gasifier operates very deficient in oxygen. This is why no high temperature peak from oxygen-rich combustion is observed in the cocurrent gasifier.

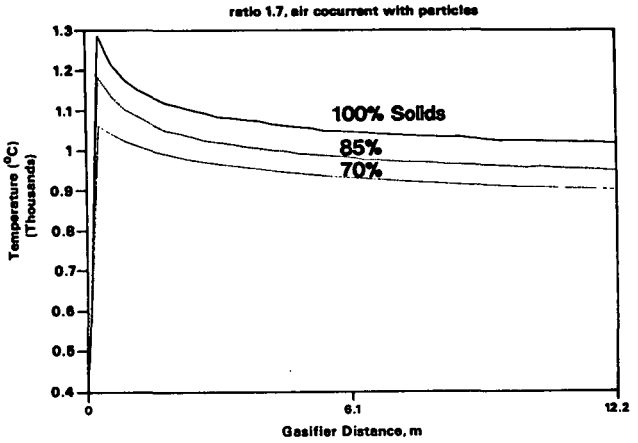

Figure 11. Effect of solids on gas temperature profiles.

Figure 11 indicates that the exit gas temperatures for 85 and 70% solids feed are 67 and 115°C lower than that for dry solids, respectively. Figure 12 shows that the HHV of exit gas for the 85 and 70% solids cases are 420 and 1100 KJ/m^3 lower than that for dry solids feed, respectively, due to incomplete gasification. For the particular gasifier length chosen, char gasification is almost complete for the dry solids feed. Substantially greater length is needed for the other two cases. About 80% of the total gas heating value is obtained within the first 20% of the gasifier length. In contrast to the countercurrent operation, the liquor solids content is an important operating parameter in cocurrent operation. An external heat source has to be supplied to achieve complete gasification of 70% solids content liquor.

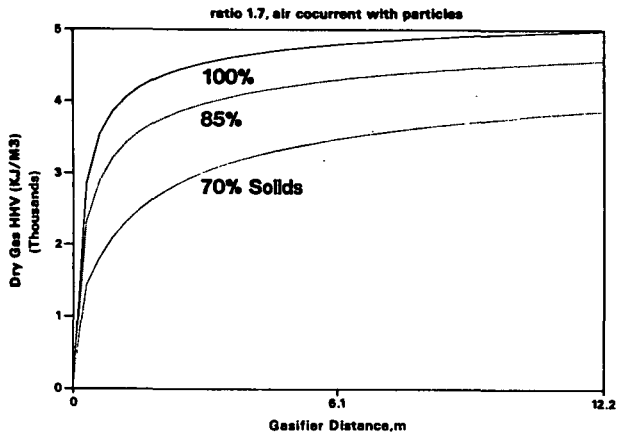

Figure 12. HHV profiles in cocurrent flow.

Figure 13 shows gas concentration profiles for dry solids at air/solids ratio of 1.7. Both CO and H_2 concentration increase monotonically with the gasifier distance, while water vapor and CO_2 concentration decrease with the gasifier distance. Equilibrium predicts that the methane concentration will be negligible, since the exit gas temperature of the cocurrent gasifier is much higher than that for the countercurrent gasifier.

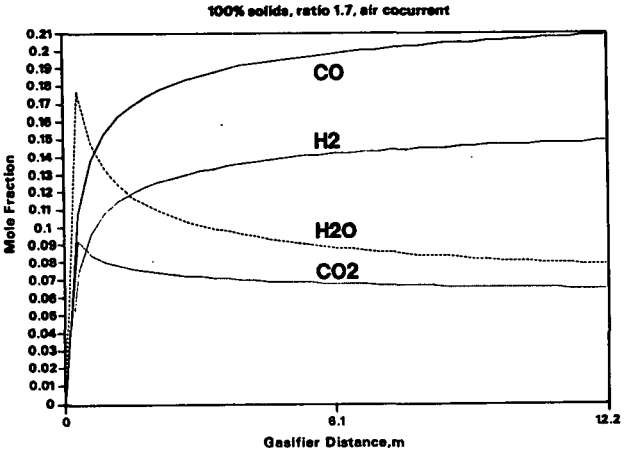

Figure 13. Gas concentration profiles.

Effect of Air/Solids Ratio

Air/liquor mass ratio was shown to be a critical parameter in determining HHV of the product gas generated in bench-scale gasifier tests at one atmosphere. Figure 14 shows the effect of air/solids ratio on temperature and HHV of the fuel gas exiting from a cocurrent gasifier run with dry solids at 15 atmospheres. The predictions of the model for the cocurrent case are compared with adiabatic equilibrium calculations in which the reaction kinetics are assumed to be infinite fast. The model predicts the exit gas to be very close to equilibrium for air/solids ratios greater than 2.0, as shown in Figure 14. For air/solids ratio below 2.0, the departure of temperature and HHV from equilibrium values becomes greater as the ratio decreases.

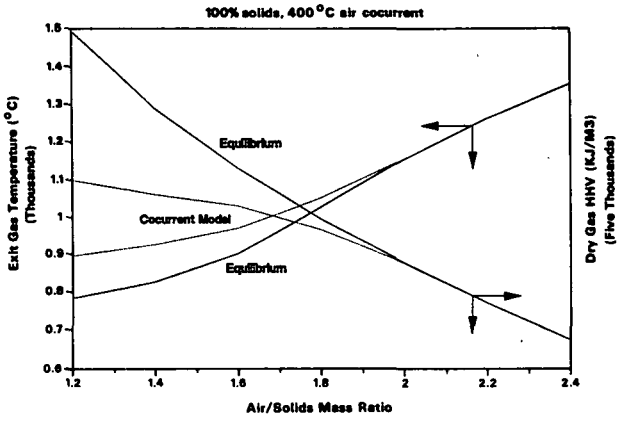

Figure 14. Effect of air/solids ratio on temperature and HHV.

For an air/solids ratio above about 1.6, the dry gas HHV decreases dramatically with increasing air/solids as predicted by equilibrium ratio. Below 1.6 the HHV is nearly independent of the air/solids ratio and much less than the equilibrium value. This must be due to incomplete gasification at low air/solids ratios. This suggests that the optimum value of air/solids ratio is around 1.7 for dry black liquor gasified in cocurrent flow with air.

It is also interesting to note that the departure from equilibrium starts at exit gas temperatures between 900 to 1000°C which is consistent with the temperature range 900-1050°C reported for the bench-scale gasifier.

Effect of Air Temperature

The effect of air temperature on HHV and exit gas temperature is shown in Figure 15 for 85% solids content feed liquor and an air/solids mass ratio of 1.7. Exit gas temperature and HHV predicted by the model are compared with those from adiabatic equilibrium calculations. The model predictions approach the equilibrium values as the air temperature increases. This is because reaction rates become faster as the temperature in the gasifier increases. The effect of air temperature on HHV diminishes at higher air temperature because the exit gas is approaching to the equilibrium at higher temperature.

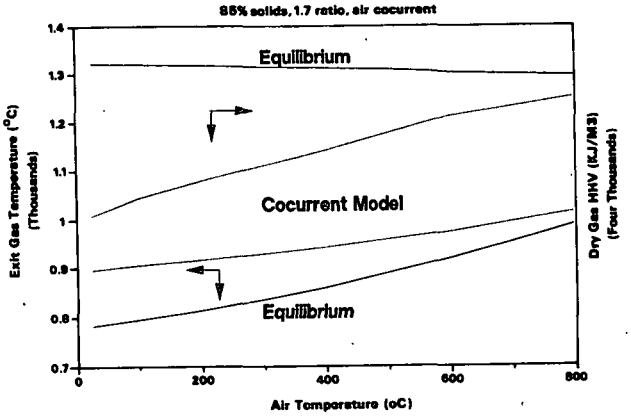

Figure 15. Effect of air temperature on HHV and gas temperature.

Sulfur and Sodium Emissions

All bench and pilot scale tests performed by Kelleher and Kohl (4,5,6,7) are at one atmosphere. There are no experimental data available now to demonstrate the effect of pressure on gasification. Figure 16 shows the sulfur and sodium emission predicted by equilibrium as a function of position along the gasifier for the cocurrent case at 15 atmospheres. The sodium emissions including sodium and sodium hydroxide vapor are predicted to be much smaller than the sulfur emissions at the higher pressure.

Equilibrium calculations show that the sulfur emission increases dramatically with the pressure, as shown in Figure 17. This can be rationalized by the following reaction:

$$Na_2S(1) + H_2O(g) + CO_2(g) \text{ <---> } H_2S(g) + Na_2CO_3(1)$$

Increasing pressure will drive the reaction to the right since there are two gas species on the left and only one on the right.

The particulate emission decreases dramatically with increasing pressure, as shown in Figure 17. This can be understood by the following reactions which shift toward the left as pressure increases:

$$Na_2CO_3(1) + CO(g) \text{ <---> } 2\ Na(g) + 2\ CO_2(g)$$

or $$Na_2CO_3(1) + H_2O(g) \text{ <---> } 2\ NaOH(g) + CO_2(g)$$

Since the sulfur emission decreases with increasing temperature and sodium emission increases with increasing temperature from equilibrium calculations, the sulfur emission increases and the sodium emission decreases along the gasifier, as shown in Figure 16.

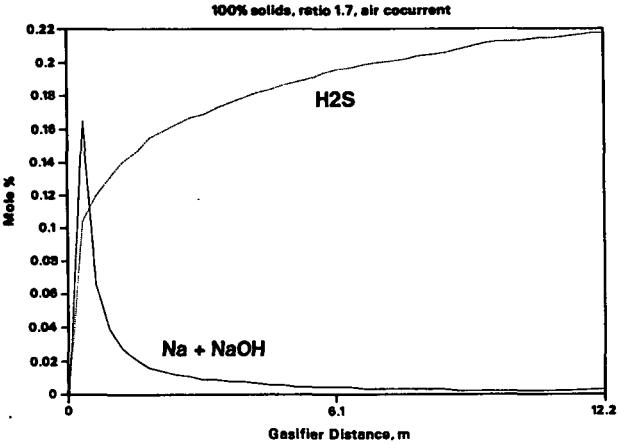

Figure 16. Sulfur and sodium emissions.

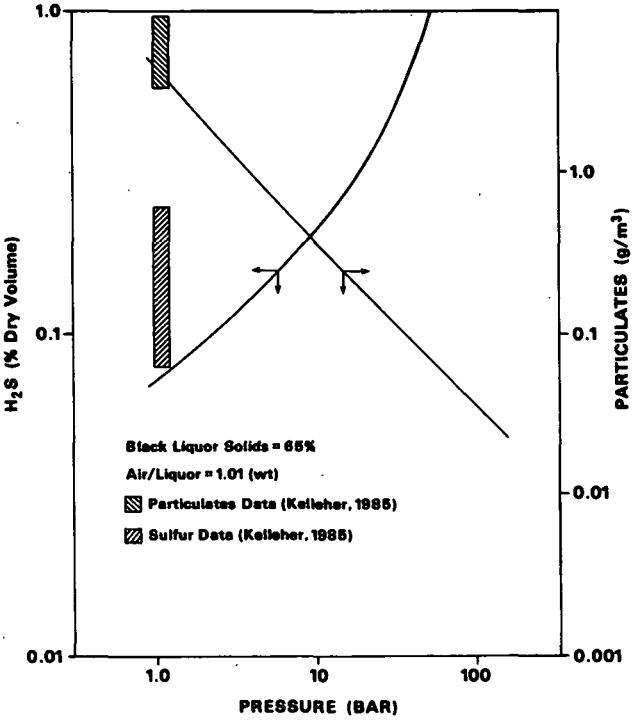

Figure 17. Sulfur and sodium emissions as function of pressure during gasification.

CONCLUSIONS

A one dimensional mathematical model for black liquor gasification was developed and used to

explore the effects of solids content, air/solids ratio, drop size and size distribution on gasifier performance for two different operating modes:

(1) Air in plug flow countercurrent to black liquor particles falling downward with diameters between 1 and 5 mm.

(2) Air in cocurrent flow with fine black liquor particles between 10 and 100 micron in diameter.

The high heating value of the exit gas in countercurrent operation is not sensitive to the solids content of black liquor which is a real advantage over the cocurrent operations. This indicates that 70% solids liquor which cannot be gasified during cocurrent operations without using either an external heat source (plasma or fossil fuel) or oxygen enriched oxidant, could be run in a countercurrent operation.

There are marked differences in the behavior and response to process variables between countercurrent and cocurrent operation. The air/solids ratio is a key parameter for both cases, but the exit gas HHV is not sensitive to the inlet liquor solids content for the countercurrent case, while it is for the cocurrent case unless an external heat source is used. The drop size and drop size distribution have a marked effect on countercurrent operation. Drop size did not affect cocurrent behavior over the range of fine particle sizes chosen.

Countercurrent operation produces a sharp peak in temperature within the gasifier and a narrow operating window for high reduction efficiency. These effects are very marked with monosized particles but are lessened with a broader particle size distribution. The oxygen consuming processes are spread out over the lower gasifier when a broader size distribution is used and the oxygen consumption by large particles in the lower gasifier protects the smaller particles from sulfide reoxidation. These types of effects are not observed in the cocurrent case.

For an air/solids ratio above 1.6 the dry gas HHV from the cocurrent gasifier decreases dramatically with increasing air/solids ratio, as predicted by equilibrium. Below 1.6 the product gas HHV is nearly independent of air/solids ratio and much less than the equilibrium value. This must be due to incomplete gasification at low air/solids ratios. This suggests that the optimum value of air/solids ratio is around 1.7 for dry black liquor gasified in cocurrent flow with air.

Equilibrium calculations for the cocurrent case predict that sulfur emissions increase with increasing pressure and decreasing temperature. The sodium emission decreases with increasing pressure and decreasing temperature. The sodium emission is predicted to be much lower than the sulfur emission, especially at the end of the cocurrent gasifier where the temperature is lowest.

LITERATURE CITED

1. Yoon, H., J. Wei and M. M. Denn. A Model for Moving-Bed Coal Gasification Reactors. AIChE J. 24(5):885 (1978).

2. Wen, C. Y. and E. S. Lee (Editors). Coal Conversion Technology. Addison-Wesley, 1979.

3. Smoot, L. D. and P. J. Smith. Coal Combustion and Gasification. Plenum Press, 1985.

4. Kelleher, E. G. Feasibility Study: Black Liquor Gasification and Use of the Products in Combined-Cycle Cogeneration. Tappi 67(4):114 (1984).

5. Kelleher, E. G. Black Liquor Gasification and Use of the Product Gases in Combined Cycle Cogeneration - Phase 2. Intl. Chem. Recovery Conf., preprints, New Orleans, April, 1985.

6. Kohl, A. L. Black Liquor Gasification. Can. J. Chem. Eng. 64(4):299 (1986).

7. Kelleher, E. G. and A. L. Kohl. Black Liquor Gasification Technology. Chemical Engineering Technology in Forest Products Processing 2:40 (1988).

8. Hupa, M., P. Solin and P. Hyoty. Combustion Behaviour of Black Liquor Droplets. Intl. Chem. Recovery Conf., New Orleans, 1985.

9. Iatridis B. and G. R. Gavalas. Pyrolysis of a Precipitated Kraft Lignin. Ind. Eng. Chem. Prod. Res. Dev. 18(2):127 (1979).

10. Clay, D. T., et al. Fundamental Studies of Black Liquor Combustion Report No. 3 - Phase 1, to DOE by The Institute of Paper Chemistry, Dec., 1987.

11. Kubes, G. J., B. I. Fleming, J. M. Macleod, and H. I. Bolker. Thermal Analysis of Spent Pulping Liquor: Activation Energies. CPPA Technical Section, Pacific Coast and Western Branches, 1981 Spring Conference.

12. Kulas, K. C. and D. T. Clay. An Empirical Equation of the Volatilization of Kraft Black Liquor During Burning. Chemical Engineering Technology in Forest Products Processing 2:53 (1988).

13. Grace, T. M., J. H. Cameron and D. T. Clay. Role of the Sulfate/Sulfide Cycle in Char Burning - Experimental Results and Implications. Intl. Chem. Recovery Conf., New Orleans, 1985.

14. Goerg, K. A. and J. H. Cameron. A Kinetic Study of Kraft Char Gasification with CO_2. Chemical Engineering Technology in Forest Products Processing 2:46 (1988).

15. Li, J. Pyrolysis and CO2 Gasification of Black Liquor Char. M. Eng. Thesis, McGill University, Montreal, 1986.

16. Wallis, G. B. One Dimensional Two Phase Flow. McGraw-Hill, New York, 1969.

17. Govind, R. and J. Shah. Modeling and Simula-

tion of an Entrained Flow Coal Gasifier. AIChE J. 30 (1):79 (1984).

18. Chase, M. W., et al. JANAF Thermochemical Tables, Third Edition, Part I and Part II. J. Phys. Chem. Ref. Data, Vol. 14, Suppl. 1, 1985.

19. Reid, R. C., J. M. Prausnitz, and T. K. Sherwood. The Properties of Gases and Liquids. 3rd Edition, McGraw-Hill, 1977.